Coupling Characteristics of Eccentric Arranged Dielectric Disk and Ring

Qing Han, *Student Member, IEEE*, Yoshinori Kogami, *Member, IEEE*, Yoshiro Tomabechi, *Member, IEEE*, and Kazuhito Matsumura, *Senior Member, IEEE*

***Abstract*—An analysis is presented for a novel coupling configuration in which a circular dielectric disk and ring are arranged eccentrically. Whispering gallery (WG) mode coupling characteristics between the dielectric disk and ring are investigated. In this paper, a coupled-mode equation based on the Lorentz's reciprocity theorem is utilized. Distributed coupling coefficients and electric field distributions around the coupling region are obtained numerically through solving the coupled-mode equation. The theory described in this paper is confirmed by comparing measured electric field distributions with calculated ones. Electromagnetic powers flowed along the disk are also calculated. It is shown that coupling quantity of the eccentric configuration would be easily controlled by changing a radius of the disk or ring. The results obtained here will be used to design a WG mode coupled resonator for millimeter wave integrated circuits.**

I. Introduction

WHISPERING gallery (WG) mode dielectric resonators have received considerable attention of many researchers of millimeter wave integrated circuits [1]–[4]. Advantages offered by this kind of resonator, such as good field concentration, high quality factor, and adoptability to integrated circuit, lead to realize excellent performance of frequency selective devices [2] in millimeter and optical wave region.

In the past several years we have studied different shaped WG mode dielectric resonators, such as a circular disk, ring, elliptic disk, and coaxial one [5]–[7]. To develop analytical approaches of the WG mode dielectric resonators, we have considered the resonators which have relatively large dimensions compared to handling wavelengths. In the studies we find that there are a lot of resonant modes existing in a large WG mode resonator and its free spectral range (FSR) is too narrow to use practically. Thus the performance of a bandpass filter using a single WG mode dielectric resonator is poor in general. To obtain better performance, a coupled resonator consisting of more than one single WG mode resonator may be used. In this way, the FSR of the coupled resonator can be expanded to the least common multiple (LCM) of the individual resonators [8].

In this paper, we propose a novel coupling configuration composed by a WG mode dielectric disk and a ring, as shown in Fig. 1. Unlike traditional configurations in which two curved dielectric waveguides are arranged in cascade or side by side [3] [9]–[11], we place the disk inside the ring to form an eccentric configuration. It is obvious that coupling quantity between the disk and ring would be easily controlled by changing the radii of the disk and/or ring. Additionally, the fact that this eccentric configuration occupies so smaller area, when compared with the same dimensional cascade arrangement, enables us to use it in integrated circuits.

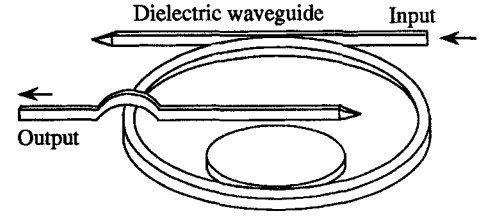

Fig. 1. Coupled dielectric resonator.

For a case of using two dielectric resonators to obtain a coupled resonator, it is the most important to understand the coupling characteristics of the coupling region. As the first step to realize the coupled resonator, we concentrate our attention to investigate the coupling characteristics between the eccentric configuration of the disk and ring.

Since the coupling characteristics depend strongly on the radii of the disk and ring, we have investigated various eccentric coupling configurations. As a result, two typical cases are given here. A coupled-mode equation of the coupling configuration is derived from the Lorentz's reciprocity theorem. Coupled electromagnetic field around the coupling mechanism is expressed by linear combination of those of individual curved guides with weight functions.

The analytical method is given in the following section. In Section III, the coupled-mode equation is solved numerically and the results of distributed coupling coefficients and electric field distributions are presented. In order to verify the theory described here, in Section IV, experiments for the same dimensional configurations as calculations are carried out. The experimental results are also compared with the theoretical ones and they show a good agreement. Finally, electromagnetic powers propagating along the disk are calculated in the Section V. As a consequence, we can expect to apply the method described here to design a better performance filter in the future.

Manuscript received July 26, 1995; revised July 22, 1996.

Q. Han, Y. Kogami, and K. Matsumura are with the Department of Electrical and electronics Engineering, Utsunomiya University, Utsunomiya 321, Japan.

Y. Tomabechi is with the Department of Education, Utsunomiya University, Utsunomiya 321, Japan.

Publisher Item Identifier S 0018-9480(96)07919-7.

II. Derivation of Coupled-Mode Equation

A. An Application of Reciprocity Theorem for WG Mode Fields in Two Media $\varepsilon_a(r,\theta,y)$ and $\varepsilon_b(r,\theta,y)$ under Cylindrical Coordinates

So far, mathematical formulations which describe two parallel and nonparallel dielectric waveguide coupling mode under rectangular coordinates have been introduced variously [12]–[15]. Although the formulation applies to nonparallel systems, it is useful only when the coupling region is small, e.g. those like two dielectric disks coupled side by side [14], [15]. However, a mathematical formulation for the coupling structure such as Fig. 1, which has a large region of dielectric proximity, has not been found. On some assumptions discussed below, we derive a new mathematical formulation under cylindrical coordinates and its validity will also be verified by comparing the calculated results with experimental ones in the later Sections. We consider two sets of the WG mode field $(\boldsymbol{E_a}, \boldsymbol{H_a})$ and $(\boldsymbol{E_b}, \boldsymbol{H_b})$ in two different media $\varepsilon_a(r,\theta,y)$ and $\varepsilon_b(r,\theta,y)$, which satisfy the Maxwell's equations and the boundary conditions. Following similar procedures for the Lorentz's reciprocity theorem [12]–[13], we obtain a relation in a cylindrical coordinates as follows

$$\nabla\cdot(\boldsymbol{E_a}\times\boldsymbol{H_b}-\boldsymbol{E_b}\times\boldsymbol{H_a}) = j\omega(\varepsilon_a(r,\theta,y)-\varepsilon_b(r,\theta,y))\boldsymbol{E_a}\cdot\boldsymbol{E_b}. \quad (1)$$

Before proceeding further with the formal mathematical manipulation, it is necessary to state the assumptions we use in the analysis.

1) The radii of curved dielectric waveguides we discussed are considerably larger than handling wavelength.
2) Electromagnetic fields are well confined in the curved dielectric waveguides.
3) The radiation loss of the dielectric waveguides is considerably small.

Taking into account the above assumptions, we can obtain the following relation after applying the (1) to an infinitesimal section $\Delta\theta$. The derivation of (2) is shown in Appendix A

$$\frac{\partial}{\partial\theta}\int_s\int\frac{1}{r}(\boldsymbol{E_a}\times\boldsymbol{H_b}-\boldsymbol{E_b}\times\boldsymbol{H_a})\cdot\hat{\theta}\,\boldsymbol{dr\,dy} = j\omega\int_s\int(\varepsilon_a(r,\theta,y)-\varepsilon_b(r,\theta,y))\boldsymbol{E_a}\cdot\boldsymbol{E_b}\,dr\,dy. \quad (2)$$

Where to keep the (2) be a function of θ the infinitesimal section $\Delta\theta$ is made substantially thin, therefore we take an area integral instead of volume integral over (1). The $\hat{}$ is symbol for a unit vector.

B. Typical Example

1) Coupling Structure and Coordinate System: Fig. 2 shows the coupling structure of a three-dimensional (3-D) circular disk and ring waveguides and the relationship between them under different coordinates. In the figure, R_1 is a radius of the disk, while R_2 and R_3 are radii of the ring. Both disk and ring have the same height of H and complex relative permittivity $\varepsilon_r = \varepsilon' - j\varepsilon''$. The relative permittivity of surrounding medium is ε_1. We now introduce two cylindrical coordinates $o_p(r_p,\theta_p,y)$ and $o_q(r_q,\theta_q,y)$ for the disk and ring, respectively , as shown in Fig. 2. For the convenience of analysis, we sometimes do not make distinctions between $o_p(r_p,\theta_p,y)$ and $o(r,\theta,y)$ in the following proceedings. For the two cylindrical coordinates mentioned above, there exist the relations between the disk and ring as follows

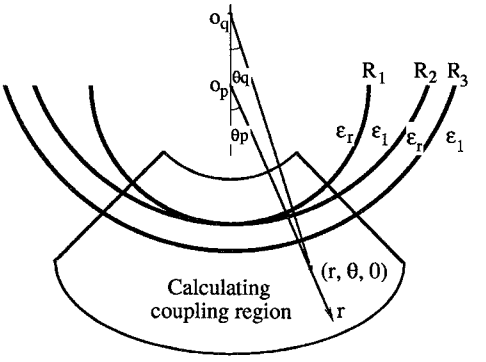

Fig. 2. Coordinate system and coupling region.

$$\begin{aligned}\hat{r}_q &= \cos(\theta-\theta_q)\hat{r}-\sin(\theta-\theta_q)\hat{\theta}\\ \hat{\theta}_q &= \sin(\theta-\theta_q)\hat{r}+\cos(\theta-\theta_q)\hat{\theta}\\ \hat{y}_q &= \hat{y} \end{aligned} \quad (3)$$

$$r_q = \sqrt{(r_p\sin\theta_p)^2+(r_p\cos\theta_p+R_2-R_1)^2}$$

$$\theta_q = \sin^{-1}\left(\frac{r_p\sin\theta_p}{r_q}\right). \quad (4)$$

When the fields of the disk are

$$\begin{aligned}\boldsymbol{E_{pt}} &= E_{yp}\hat{y}\\ \boldsymbol{H_{pt}} &= H_{rp}\hat{r}\\ \boldsymbol{E_{p\theta}} &= E_{\theta p}\hat{\theta}\\ \boldsymbol{H_{p\theta}} &= H_{\theta p}\hat{\theta}\end{aligned} \quad (5)$$

using (3) and (4), we can express the fields of the ring under the disk's coordinates as

$$\begin{aligned}\boldsymbol{E_{qt}} &= \sin(\theta-\theta_q)E_{\theta q}\hat{r}+E_{yq}\hat{y}\\ \boldsymbol{H_{qt}} &= (\sin(\theta-\theta_q)H_{\theta q}+\cos(\theta-\theta_q)H_{rq})\hat{r}\\ \boldsymbol{E_{q\theta}} &= \cos(\theta-\theta_q)E_{\theta q}\hat{\theta}\\ \boldsymbol{H_{q\theta}} &= (-\sin(\theta-\theta_q)H_{rq}+\cos(\theta-\theta_q)H_{\theta q})\hat{\theta}\end{aligned} \quad (6)$$

where t and θ indicate the transverse and longitudinal components, respectively. The symbols $\boldsymbol{E_{yp}}, \boldsymbol{H_{rp}}, \boldsymbol{E_{\theta p}}, \boldsymbol{H_{\theta p}}, \boldsymbol{E_{yq}}, \boldsymbol{H_{rq}}, \boldsymbol{E_{\theta q}}, \boldsymbol{H_{\theta q}}$ given in [5] are solutions for the fields in the isolated disk and ring and are also rewritten in the Appendix B. According to WG mode nomenclature, these solutions belong to WGH mode [4].

2) Coupled-Mode Equation: As shown in Fig. 3 (a), (b), and (c), we suppose the functions $\varepsilon_p(r,\theta,y)$ and $\varepsilon_q(r,\theta,y)$ represent the variation in the relative permittivities when only the disk and ring are presented, respectively, i.e.,

$$\varepsilon_{p,q}(r,\theta,y) = \begin{cases}\varepsilon_{p,q}; & \text{within the guides}\\ \varepsilon_1; & \text{otherwise}\end{cases} \quad (7)$$

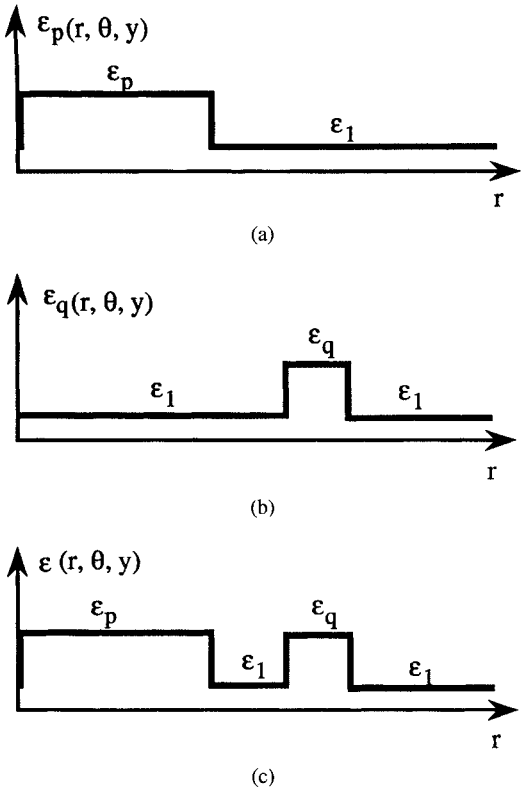

Fig. 3. Relative permittivities for (a) $\varepsilon_p(r,\theta,y)$ with a single disk, (b) $\varepsilon_q(r,\theta,y)$ with a single ring, (c) $\varepsilon(r,\theta,y)$ with both disk and ring.

where $\varepsilon_p(r,\theta,y) = \varepsilon_1\,(\text{not}\,\varepsilon_q)$ in the region ring occupies and vice versa. The function $\tilde{\varepsilon}(r,\theta,y)$ represents the relative permittivity when both disk and ring exist simultaneously. According to the coupled-mode theory [13]–[16], we express total coupled fields $(\boldsymbol{E_c}, \boldsymbol{H_c})$ around the coupling region by linear combination of modal fields $(\boldsymbol{E_{1,2}}, \boldsymbol{H_{1,2}})$ of the individual waveguides with weight functions $m_p(\theta), m_q(\theta)$. We also note that the following expansion is only an approximate set of solutions to the Maxwell equations in the coupled-waveguide medium $\tilde{\varepsilon}(r,\theta,y)$ and the radiation mode has been neglected

$$\begin{aligned}\boldsymbol{E_c}(\boldsymbol{r},\theta,\boldsymbol{y}) &= m_p(\theta)\boldsymbol{E_1}(\boldsymbol{r},\theta,\boldsymbol{y}) \\ &\quad + \boldsymbol{m_q}(\theta)\boldsymbol{E_2}(\boldsymbol{r},\theta,\boldsymbol{y}) \\ &\simeq m_p(\theta)\exp[-j(\beta_p - j\alpha_p)R_p\theta_p] \\ &\quad \cdot \left(\boldsymbol{E_{pt}} + \frac{\varepsilon_{\boldsymbol{p}}(\boldsymbol{r},\theta,\boldsymbol{y})}{\tilde{\varepsilon}(\boldsymbol{r},\theta,\boldsymbol{y})}\boldsymbol{E_{p\theta}}\hat{\theta}\right) \\ &\quad + m_q(\theta)\exp[-j(\beta_q - j\alpha_q)R_q\theta_q] \\ &\quad \cdot \left(\boldsymbol{E_{qt}} + \frac{\varepsilon_{\boldsymbol{q}}(\boldsymbol{r},\theta,\boldsymbol{y})}{\tilde{\varepsilon}(\boldsymbol{r},\theta,\boldsymbol{y})}\boldsymbol{E_{q\theta}}\hat{\theta}\right) \qquad (8a)\end{aligned}$$

$$\begin{aligned}\boldsymbol{H_c}(\boldsymbol{r},\theta,\boldsymbol{y}) &= m_p(\theta)\boldsymbol{H_1}(\boldsymbol{r},\theta,\boldsymbol{y}) \\ &\quad + \boldsymbol{m_q}(\theta)\boldsymbol{H_2}(\boldsymbol{r},\theta,\boldsymbol{y}) \\ &\simeq m_p(\theta)\exp[-j(\beta_p - j\alpha_p)R_p\theta_p](\boldsymbol{H_{pt}} + \boldsymbol{H_{p\theta}}\hat{\theta}) \\ &\quad + m_q(\theta)\exp[-j(\beta_q - j\alpha_q)R_q\theta_q] \\ &\quad \cdot (\boldsymbol{H_{qt}} + \boldsymbol{H_{q\theta}}\hat{\theta}) \qquad (8b)\end{aligned}$$

where $\boldsymbol{E_{1,2}}$ and $\boldsymbol{H_{1,2}}$ which propagate in the $+\theta$ direction are the mode fields each guide supports if the other guide is not there. The $\beta_{p,q}$ and $\alpha_{p,q}$ are their phase and attenuation constants. The derivation of longitudinal components appeared in (8a) are shown in Appendix C. On the other hand, the modal fields propagating along the $-\theta$ direction of the isolated disk and ring can be written respectively, as follows

$$\begin{aligned}\boldsymbol{E_1^-}(r,\theta,y) &\simeq \exp[j(\beta_p - j\alpha_p)R_p\theta_p](\boldsymbol{E_{pt}} - \boldsymbol{E_{p\theta}}\hat{\theta}) \\ \boldsymbol{H_1^-}(r,\theta,y) &\simeq \exp[j(\beta_p - j\alpha_p)R_p\theta_p](-\boldsymbol{H_{pt}} + \boldsymbol{H_{p\theta}}\hat{\theta}) \qquad (9a) \\ \boldsymbol{E_2^-}(r,\theta,y) &\simeq \exp[j(\beta_q - j\alpha_q)R_q\theta_q](\boldsymbol{E_{qt}} - \boldsymbol{E_{q\theta}}\hat{\theta}) \\ \boldsymbol{H_2^-}(r,\theta,y) &\simeq \exp[j(\beta_q - j\alpha_q)R_q\theta_q](-\boldsymbol{H_{qt}} + \boldsymbol{H_{q\theta}}\hat{\theta}) \qquad (9b)\end{aligned}$$

where, superscript $^-$ indicates the $-\theta$ direction.

For the purpose of deriving coupled-mode equations, two sets of electromagnetic fields are necessary by using reciprocity relation (2). We choose the total coupled fields shown in (8a) and (8b) as the first set of solutions. For the second set, we choose individual modal fields which propagate in the $-\theta$ direction. That is, we get coupled-mode equation (10) when we choose $\boldsymbol{E_c}, \boldsymbol{H_c}$ (8a,b) and $\boldsymbol{E_1^-}, \boldsymbol{H_1^-}$ (9a); we get (11) when we choose $\boldsymbol{E_c}, \boldsymbol{H_c}$ (8a,b) and $\boldsymbol{E_2^-}, \boldsymbol{H_2^-}$ (9b)

$$\begin{aligned}&\frac{\partial}{\partial\theta}\left\{m_p(\theta)\int_{-\infty}^{\infty}\int_0^{\infty}\frac{2}{\omega\varepsilon_0 r}(\boldsymbol{E_{pt}}\times\boldsymbol{H_{pt}})\cdot\hat{\theta}\,\boldsymbol{dr}\,\boldsymbol{dy}\right\} \\ &\quad + \frac{\partial}{\partial\theta}\left\{m_q(\theta)\int_{-\infty}^{\infty}\int_0^{\infty}\frac{\exp(j\nu_p\theta_p - j\nu_q\theta_q)}{\omega\varepsilon_0 r}\right. \\ &\quad \left.\cdot(\boldsymbol{E_{qt}}\times\boldsymbol{H_{pt}} + \boldsymbol{E_{pt}}\times\boldsymbol{H_{qt}})\cdot\hat{\theta}\,\boldsymbol{dr}\,\boldsymbol{dy}\right\} \\ &= -jm_p(\theta)\int_{-\infty}^{\infty}\int_0^{\infty}(\tilde{\varepsilon}(r,\theta,y) - \varepsilon_p(r,\theta,y)) \\ &\quad \cdot\left(\boldsymbol{E_{pt}}\cdot\boldsymbol{E_{pt}} - \frac{\varepsilon_{\boldsymbol{p}}(\boldsymbol{r},\theta,\boldsymbol{y})}{\tilde{\varepsilon}(\boldsymbol{r},\theta,\boldsymbol{y})}\boldsymbol{E_{p\theta}^2}\right)dr\,dy \\ &\quad - jm_q(\theta)\int_{-\infty}^{\infty}\int_0^{\infty}(\tilde{\varepsilon}(r,\theta,y) - \varepsilon_p(r,\theta,y)) \\ &\quad \cdot\exp(j\nu_p\theta_p - j\nu_q\theta_q) \\ &\quad \cdot\left(\boldsymbol{E_{qt}}\cdot\boldsymbol{E_{pt}} - \frac{\varepsilon_{\boldsymbol{q}}(\boldsymbol{r},\theta,\boldsymbol{y})}{\tilde{\varepsilon}(\boldsymbol{r},\theta,\boldsymbol{y})}\boldsymbol{E_{q\theta}}\boldsymbol{E_{p\theta}}\right)dr\,dy \qquad (10)\end{aligned}$$

$$\begin{aligned}&\frac{\partial}{\partial\theta}\left\{m_p(\theta)\int_{-\infty}^{\infty}\int_0^{\infty}\frac{\exp[-(j\nu_p\theta_p - j\nu_q\theta_q)]}{\omega\varepsilon_0 r}\right. \\ &\quad \left.\cdot(\boldsymbol{E_{pt}}\times\boldsymbol{H_{qt}} + \boldsymbol{E_{qt}}\times\boldsymbol{H_{pt}})\cdot\hat{\theta}\,\boldsymbol{dr}\,\boldsymbol{dy}\right\} \\ &\quad + \frac{\partial}{\partial\theta}\left\{m_q(\theta)\int_{-\infty}^{\infty}\int_0^{\infty}\frac{2}{\omega\varepsilon_0 r}(\boldsymbol{E_{qt}}\times\boldsymbol{H_{qt}})\cdot\hat{\theta}\,\boldsymbol{dr}\,\boldsymbol{dy}\right\} \\ &= -jm_p(\theta)\int_{-\infty}^{\infty}\int_0^{\infty}(\tilde{\varepsilon}(r,\theta,y) - \varepsilon_q(r,\theta,y)) \\ &\quad \cdot\exp[-(j\nu_p\theta_p - j\nu_q\theta_q)] \\ &\quad \cdot\left(\boldsymbol{E_{pt}}\cdot\boldsymbol{E_{qt}} - \frac{\varepsilon_{\boldsymbol{p}}(\boldsymbol{r},\theta,\boldsymbol{y})}{\tilde{\varepsilon}(\boldsymbol{r},\theta,\boldsymbol{y})}\boldsymbol{E_{p\theta}}\boldsymbol{E_{q\theta}}\right)dr\,dy \\ &\quad - jm_q(\theta)\int_{-\infty}^{\infty}\int_0^{\infty}(\tilde{\varepsilon}(r,\theta,y) - \varepsilon_q(r,\theta,y)) \\ &\quad \cdot\left(\boldsymbol{E_{qt}}\cdot\boldsymbol{E_{qt}} - \frac{\varepsilon_{\boldsymbol{q}}(\boldsymbol{r},\theta,\boldsymbol{y})}{\tilde{\varepsilon}(\boldsymbol{r},\theta,\boldsymbol{y})}\boldsymbol{E_{q\theta}^2}\right)dr\,dy \qquad (11)\end{aligned}$$

where

$$\begin{aligned}&\exp[\pm(j\nu_p\theta_p - j\nu_q\theta_q)] \\ &\quad = \exp[\pm j\{(\beta_p - j\alpha_p)R_p\theta_p - (\beta_q - j\alpha_q)R_q\theta_q\}]\end{aligned}$$

TABLE I
DIMENSIONS OF THE DISK AND RING

$f_0 = 24$ GHz, $\varepsilon_r = 2.01 - j\,8.643\times10^{-4}$, $\varepsilon_1 = 1.0$, H = 8 mm

CASE1	CASE2
$R_1 = 10.0$ cm	$R_1 = 10.0$ cm
$R_2 = 11.2$ cm	$R_2 = 20.0$ cm
$R_3 = 12.0$ cm	$R_3 = 20.8$ cm
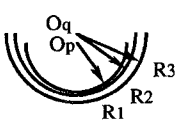	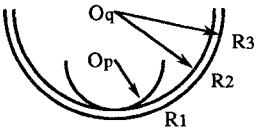

is propagating factor of the coupled mode. Equation (10) and (11) can be regarded as simultaneous differential equation form and rewritten as a matrix form. Therefore, for the weight functions $m_p(\theta), m_q(\theta)$, we have

$$\begin{bmatrix} \dfrac{\partial m_p(\theta)}{\partial \theta} \\ \dfrac{\partial m_q(\theta)}{\partial \theta} \end{bmatrix} = \begin{bmatrix} k_{pp}(\theta) & k_{pq}(\theta) \\ k_{qp}(\theta) & k_{qq}(\theta) \end{bmatrix} \begin{bmatrix} m_p(\theta) \\ m_q(\theta) \end{bmatrix} \tag{12}$$

where $k_{ij}(i, j = p, q)$ indicate coupling coefficients which are complex values, and vary with θ direction.

III. Numerical Results

A. Dimensions of Calculation

Since the coupling characteristics depend very strongly on the radii of the disk and ring, it is necessary to investigate various cases of eccentric configuration. In this paper we discuss two typical examples, i.e., for a fixed disk, radii of the ring are changed relative smaller and larger. From now on we call these two examples as CASE1 and CASE2, respectively. The dimensions and dielectric constants used in calculations are summarized in the Table I. The coupling range considered in this paper is $-\pi/4[\text{rad.}] < \theta < \pi/4[\text{rad.}]$ in θ direction.

B. Distributed Coupling Coefficients

Putting the integrals in (10) and (11) into practice, we show the coupling coefficients $\kappa_{ij}(i, j = p, q)$ between the disk and ring in Fig. 4, where $\kappa_{ij} = k_{ij}/(-j)$. Unlike parallel coupling cases, eccentric coupling structure gives the complex coupling coefficients varying with propagating direction. Corresponding to the coupling structures shown in the Table I, the CASE1 are more closely matched and has greater region of dielectric proximity , so that its coupling range is longer than that of the CASE2. For the example of here the coupling range of the CASE1 is at least 0.4 rad. longer than the CASE2 in terms of angles. As a consequence, we can easily control the coupling quantity between disk and ring by changing the radii of the disk and/or ring.

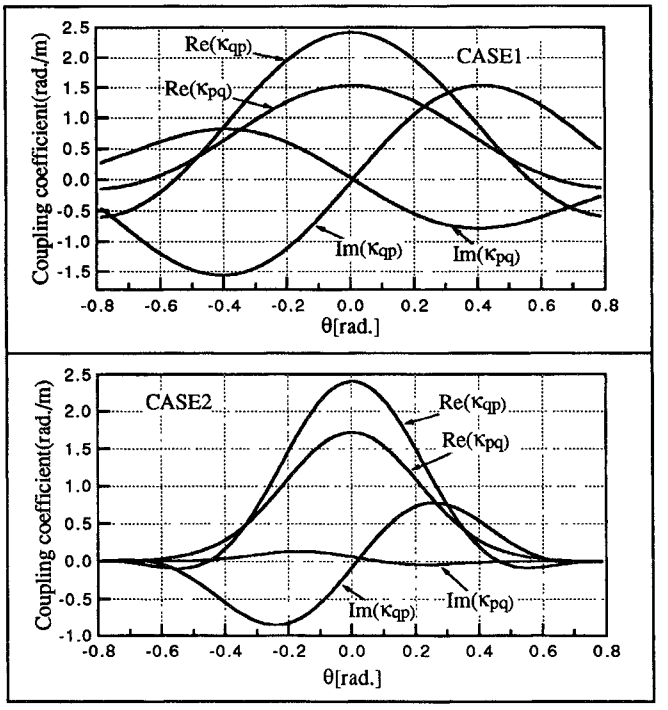

Fig. 4. Coupling coefficients of calculation.

C. Coupled Field Distributions

Solving the coupled-mode equation (12) by means of the results of the integrals in (10) and (11), we can obtain weight functions $m_p(\theta)$ and $m_q(\theta)$ numerically. Here, initial conditions $m_p(-\pi/4) = 0, m_q(-\pi/4) = 1.0 + j0$, which mean the ring is excited, are used. Then the coupled electric field distributions around the coupling region can be determined by substituting $m_p(\theta)$ and $m_q(\theta)$ into (8a). The results of coupled electric field distribution, shown in Fig. 5, are drawn using contour lines and the separations between two lines are 2.5 dB. It is obvious that CASE1 yields a very distinct result from that of CASE2. We can see that the electric field appears also in the disk region with the increasing of z at the condition which ring is excited.

IV. Experiment

In order to verify the theory derived in this paper, experimental works have been carried out at 24 GHz. Fig. 6 shows a coupling structure and an experimental set-up for measuring electromagnetic field distribution. The employed coupling structures have the same dimensions and the same material as calculated ones. A monopole antenna is controlled by an XY stage to pick up the strength of electromagnetic field. The strength at each point is measured by a network analyzer. A desktop computer is used to control the analyzer and the stage. The measurement is performed automatically. It is easy to find that the experimental results of coupled electric field distribution shown in Fig. 7 are in a good agreement with the theoretical ones shown in Fig. 5.

V. Calculation of the Power

By multiplying the electrical field component extracted from (8a) with intrinsic magnetic field of the disk and/or ring,

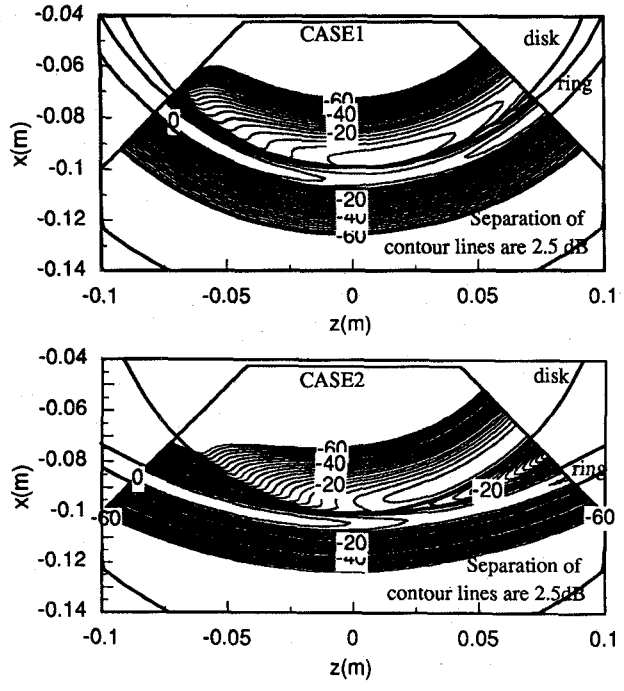

Fig. 5. Theoretical result of electric field distribution of the coupled system (ring is excited).

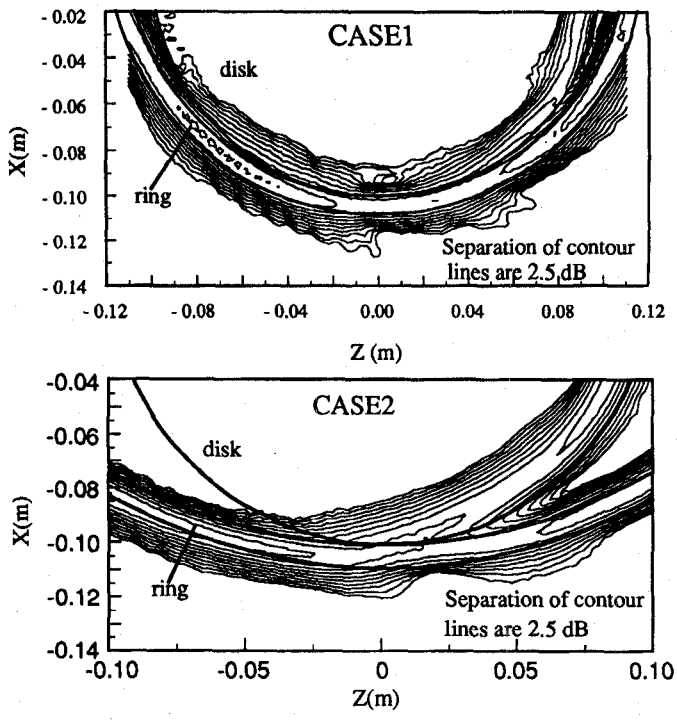

Fig. 7. Experimental result of electric field distribution of the coupled system (ring is excited).

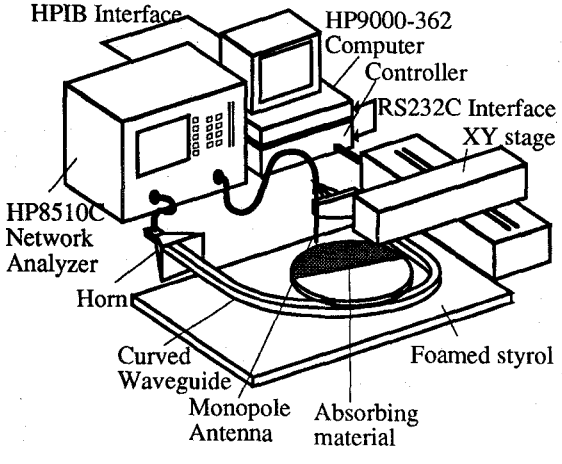

Fig. 6. The coupling part and experimental set-up for measuring electric field distribution.

we can get modal amplitude first of all. Then the power propagating along the disk and/or ring can be obtained from this modal amplitude. As an example, the modal amplitude on the disk when the disk is excited can be written as

$$A_p = \int_{-\infty}^{\infty}\int_{0}^{\infty} \{m_p(\theta)\exp[-j(\beta_p - j\alpha_p)R_p\theta_p]E_{yp}\hat{y} + m_q(\theta)\exp[-j(\beta_q - j\alpha_q)R_q\theta_q]E_{yq}\hat{y}\} \times H_{rp}\hat{r}\cdot\hat{\theta}\, dr\, dy. \quad (13)$$

Therefore the power propagating along the disk can be obtained as follows:

$$P_p = \frac{|A_p|^2}{4}. \quad (14)$$

In Fig. 8, we give the results of the propagating power along the disk when the disk is excited (solid line) and those of the power transferred to disk from the ring when the ring is excited (dashed line) in decibel. Resulting from closely matched radii or a greater dielectric proximity, the propagating power of the CASE1 behaves more changeable than that of the CASE2. Take the case of solid line in CASE1, there is a decrease to 5 dB in the region of -0.8 rad. $< \theta < 0.2$ rad., which implies the propagating power of the disk transfers into the ring. The solid line then rise to 0 dB again in 0.2 rad. $< \theta < 0.8$ rad., which implies the propagating power goes back to the disk from the ring. The other hand, the powers of the CASE2 remain stable after passing the small coupling region.

VI. Conclusion

The analytical method for coupling characteristics of the dielectric disk and ring in eccentric configuration is developed. The coupled-mode equation is established from the Lorentz's reciprocity theorem. Through solving the coupled-mode equation, we can calculate the distributed coupling coefficients and coupled electric field distributions around the coupling region accurately. The measured coupled field distributions are in a good agreement with calculated ones. The electromagnetic powers propagating along the disk are also calculated. As a result, that adequate coupling quantity between the disk and ring can be expected from this eccentric configuration enables us to utilize it to many applications. The proper analytical approach presented in this paper will be applied to design an eccentric configuration coupled resonator having the large FSR characteristic. Furthermore, the coupled resonator would be used for a high performance filter at millimeter wave band in the near future.

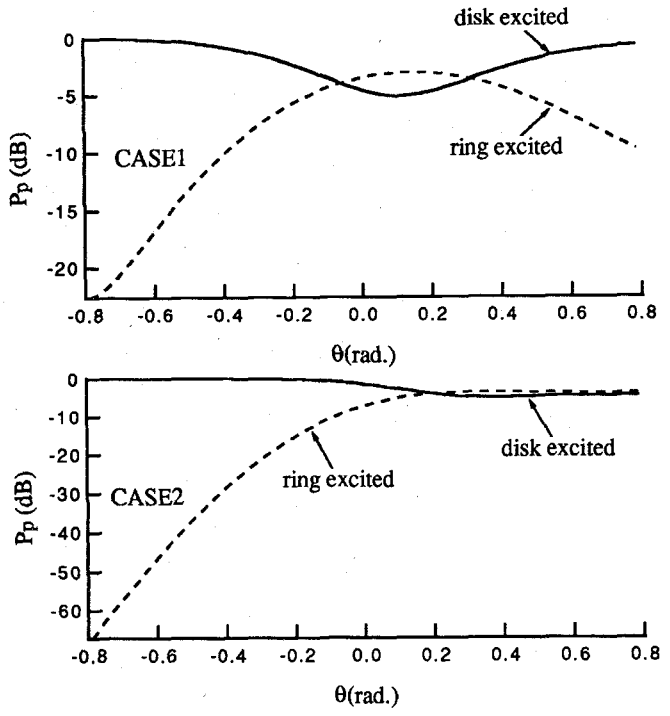

Fig. 8. The powers propagating along the disk when disk and ring is excited, respectively.

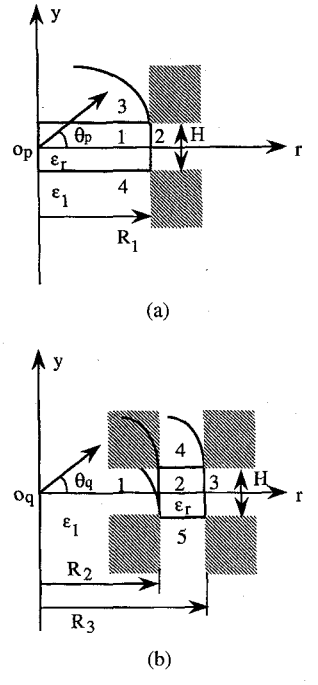

Fig. 9. (a) Dielectric disk and coordinate system. (b) Dielectric ring and coordinate system.

APPENDIX A
DERIVATION OF RECIPROCITY RELATION (2)

For a vector $\boldsymbol{A} = \hat{\boldsymbol{r}}\boldsymbol{A_r} + \hat{\theta}\boldsymbol{A}_\theta + \hat{\boldsymbol{y}}\boldsymbol{A_y}$ in cylindrical coordinates, we define

$$\nabla \cdot \boldsymbol{A} = \left(\nabla_{\boldsymbol{t}} + \frac{1}{\boldsymbol{r}}\hat{\theta}\frac{\partial}{\partial\theta}\right) \cdot \boldsymbol{A} \tag{A1}$$

as we consider circular propagating mode i.e., WG mode in the paper, $\hat{\theta}$ represents a unit vector in longitudinal direction and t represents a transverse component, i.e.,

$$\nabla_t \cdot \boldsymbol{A} = \frac{1}{\boldsymbol{r}}\frac{\partial(\boldsymbol{rA_r})}{\partial \boldsymbol{r}} + \frac{\partial \boldsymbol{A_y}}{\partial \boldsymbol{y}}.$$

Using the vector identity (A1) [12] over a cross section in the transverse plane, we have

$$\begin{aligned}\iint_s \nabla \cdot \boldsymbol{A}\, \boldsymbol{ds} &= \iint_s \left(\nabla_t + \frac{1}{r}\hat{\theta}\frac{\partial}{\partial\theta}\right) \cdot \boldsymbol{A}\, \boldsymbol{ds} \\ &= \iint_s \nabla_t \cdot \boldsymbol{A}\, \boldsymbol{ds} + \iint_{\boldsymbol{s}} \frac{1}{\boldsymbol{r}}\frac{\partial \boldsymbol{A}}{\partial\theta} \cdot \hat{\theta}\, \boldsymbol{ds}\end{aligned} \tag{A2}$$

where S is an area in the r, y plane. Keeping the assumptions $1 \sim 3$ as stated in the text in mind, we do the integration of (A2) by considering the vector $\boldsymbol{A}$ to be the electromagnetic fields of the WG mode. According to the classification of the WG mode [4], here, we take the WGH mode as an example. For the WGH mode, there exists the fields of $\boldsymbol{Ey}, \boldsymbol{H_r}, \boldsymbol{E}_\theta, \boldsymbol{H}_\theta, \boldsymbol{E_r}$ and $\boldsymbol{Hy}$. Among them, only the $(\boldsymbol{Ey} \times \boldsymbol{H_r})$ gives a strong power which propagates along the θ direction. $(\boldsymbol{E}_\theta \times \boldsymbol{Hy})$ and $(\boldsymbol{E}_\theta \times \boldsymbol{H_r})$ are remarkably weak compared to the $(\boldsymbol{Ey} \times \boldsymbol{H_r})$. Therefore, the first integration of (A2) on the right-hand is approximately zero. The similar procedure can also be applied to WGE mode

$$\iint_s \nabla_t \cdot \boldsymbol{A}\, \boldsymbol{ds} \approx 0. \tag{A3}$$

Substituting the vector $\boldsymbol{E_a} \times \boldsymbol{H_b} - \boldsymbol{E_b} \times \boldsymbol{H_a}$ into (A2) and using the condition of (A3), for (1) which discussed in the text, we have

$$\begin{aligned}\frac{\partial}{\partial\theta}\iint_s \frac{1}{r}(\boldsymbol{E_a} \times \boldsymbol{H_b} - \boldsymbol{E_b} \times \boldsymbol{H_a}) \cdot \hat{\theta}\, \boldsymbol{dr}\, \boldsymbol{dy} \\ = j\omega \iint_s (\varepsilon_a(r,\theta,y) - \varepsilon_b(r,\theta,y))\boldsymbol{E_a} \cdot \boldsymbol{E_b}\, dr\, dy\end{aligned}$$

which is a differential equation varying with θ.

APPENDIX B
WGH MODE FIELDS OF DIELECTRIC DISK AND RING

The E_{yp} components of dielectric disk for different areas [Fig. 9(a)] are written as follows:

Area 1:

$$E_{yp} = C_1 J_{\nu_p}(\sigma_p r)\cos(k_{y_p} y)\exp(-j\nu_p\theta_p).$$

Area 2:

$$E_{yp} = C_2 H^{(2)}_{\nu_p}(\rho_p r)\cos(k_{y_p} y)\exp(-j\nu_p\theta_p).$$

Area 3, 4:

$$E_{yp} = C_1 J_{\nu_p}(\sigma_p r)\exp(\mp\gamma_p y)\exp(-j\nu_p\theta_p).$$

The other components of electromagnetic fields can be derived from Maxwell's equations.

Similarly , the E_{yq} components of dielectric ring for different areas [Fig. 9(b)] are as follows:
Area 1:

$$E_{yq} = D_1 J_{\nu_q}(\rho_q r)\cos(k_{y_q} y)\exp(-j\nu_q\theta_q).$$

Area 2:

$$E_{yq} = (D_2 J_{\nu_q}(\sigma_q r) + D_3 N_{\nu_q}(\sigma_q r)). \cdot \cos(k_{y_q} y)\exp(-j\nu_q\theta_q).$$

Area 3:

$$E_{yq} = (D_4 H^{(2)}_{\nu_q}(\rho_q r)\cos(k_{y_q} y)\exp(-j\nu_q\theta_q).$$

Area 4, 5:

$$E_{yq} = (D_2 J_{\nu_q}(\sigma_q r) + D_3 N_{\nu_q}(\sigma_q r)) \cdot \exp(\mp\gamma_q y)\exp(-j\nu_q\theta_q)$$

where

$$\sigma_{p,q} = \sqrt{k_0^2\varepsilon_1 + \gamma_{p,q}^2} \quad \text{and} \quad \rho_{p,q} = \sqrt{k_0^2\varepsilon_1 - k_{y_p,y_q}^2}.$$

J_ν, N_ν and $H_\nu^{(2)}$ are Bessel, Neumann, and Hankel function, respectively. In the analysis, we assume that the electromagnetic fields are well confined in the disk and ring and the fields of shaded region in Fig. 9(a) and (b) are ignored.

APPENDIX C
DERIVATION OF LONGITUDINAL COMPONENTS IN (8a)

Similarly to Appendix A, for a vector $\boldsymbol{A} = \hat{\boldsymbol{r}}\boldsymbol{A_r} + \hat{\theta}\boldsymbol{A}_\theta + \hat{\boldsymbol{y}}\boldsymbol{A_y}$ in cylindrical coordinates, we define

$$\nabla \times \boldsymbol{A} = \left(\nabla_{\boldsymbol{t}} + \frac{1}{\boldsymbol{r}}\hat{\theta}\frac{\partial}{\partial\theta}\right) \times \boldsymbol{A} \tag{C1}$$

where t and θ indicate the transverse and longitudinal components, respectively. Using the relation of (C1), we have, for the guided modes

$$\nabla_t \times \boldsymbol{E_1} - \boldsymbol{j}\omega\mu\boldsymbol{H_1} = -\frac{1}{\boldsymbol{r}}\frac{\partial}{\partial\theta}\hat{\theta} \times \boldsymbol{E_1} \tag{C2}$$

$$\nabla_t \times \boldsymbol{H_1} + \boldsymbol{j}\omega\varepsilon\boldsymbol{E_1} = -\frac{1}{\boldsymbol{r}}\frac{\partial}{\partial\theta}\hat{\theta} \times \boldsymbol{H_1} \tag{C3}$$

and a similar set of equations for $\varepsilon_q(r,\theta,y), \boldsymbol{E_2}, \boldsymbol{H_2}$ For the coupled-waveguide medium, we have

$$\nabla_{\boldsymbol{t}} \times \boldsymbol{E} - \boldsymbol{j}\omega\mu\boldsymbol{H} = -\frac{1}{\boldsymbol{r}}\frac{\partial}{\partial\theta}\hat{\theta} \times \boldsymbol{E} \tag{C4}$$

$$\nabla_{\boldsymbol{t}} \times \boldsymbol{H} + \boldsymbol{j}\omega\varepsilon\boldsymbol{E} = -\frac{1}{\boldsymbol{r}}\frac{\partial}{\partial\theta}\hat{\theta} \times \boldsymbol{H}. \tag{C5}$$

Breaking the (C5) into the transverse and longitudinal components and just paying attention to the θ components, we have

$$\begin{aligned}\boldsymbol{E}_\theta &= -\frac{1}{\boldsymbol{j}\omega\tilde{\varepsilon}(\boldsymbol{r},\theta,\boldsymbol{y})}\nabla_{\boldsymbol{t}} \times \boldsymbol{H_t} \\ &= -\frac{1}{j\omega\tilde{\varepsilon}(r,\theta,y)}\nabla_t \times (m_p(\theta)\boldsymbol{H_{pt}} + \boldsymbol{m_q}(\theta)\boldsymbol{H_{qt}}) \\ &= -\frac{1}{j\omega\tilde{\varepsilon}(r,\theta,y)}(m_p(\theta)\nabla_t \times \boldsymbol{H_{pt}} + m_q(\theta)\nabla_t \times \boldsymbol{H_{qt}}) \\ &= -\frac{1}{j\omega\tilde{\varepsilon}(r,\theta,y)}(m_p(\theta)(-j\omega\varepsilon_p(r,\theta,y)\boldsymbol{E_{p\theta}}) \\ &\quad + m_q(\theta)(-j\omega\varepsilon_q(r,\theta,y)\boldsymbol{E_{q\theta}})) \\ &= m_p(\theta)\frac{\varepsilon_p(r,\theta,y)}{\tilde{\varepsilon}(r,\theta,y)}\boldsymbol{E_{p\theta}} + m_q(\theta)\frac{\varepsilon_q(r,\theta,y)}{\tilde{\varepsilon}(r,\theta,y)}\boldsymbol{E_{q\theta}}. \end{aligned} \tag{C6}$$

Here, E_θ is the sum of longitudinal components of disk and ring in (8a). A similar procedure can be applied to H_θ.

REFERENCES

[1] J. R. Wait, "Electromagnetic Whispering-Gallery modes in a dielectric rod," *Radio Sci.*, vol. 2, no. 9, pp. 1005–1017, Sept. 1967.
[2] C. Vedrenne and J. Arnaud, "Whispering-Gallery modes of dielectric resonators," *IEE Proc.*, vol. 129, pt. H, pp. 183–187, no. 4, Aug. 1982.
[3] X. H. Jiao and P. Guillon, "On the feasibility of millimeter wave directional filters using dielectric resonators," in *18th European Microwave Conf. Proc.*, Sept. 1988, pp. 675–680.
[4] D. Cros and P. Guillon, "Whispering gallery dielectric resonator modes for W-band devices," *IEEE Trans. Microwave Theory Tech.*, vol. 38, no. 11, pp. 1667–1674, Nov. 1990.
[5] Y. Tomabechi. and K. Matsumura, "Resonance characteristics of whispering gallery modes on a dielectric disk," (in Japanese), *Trans. IEICE*, C-I, vol. J75-C-I, no. 11, pp. 687–693, Nov. 1992.
[6] K. Matsumura, K. Shiraishi, and I. Okada, "Whispering gallery modes in an elliptic dielectric disk for millimeter through optical wave application," in *23rd European Microwave Conf. Proc.*, vol. 2, Sept. 1993, pp. 608–610.
[7] Q. Han, Y. Kogami, Y. Tomabechi, and K. Matsumura, "Resonance characteristics of circularly propagating mode in a coaxial dielectric resonator," *IEICE Trans. Electron*, vol. E77-C, no. 11, pp. 1747–1751, Nov. 1994.
[8] K. Matsumura and N. Ohki, "Dielectric dual ring resonator for millimeter through optical wave integrated circuit," in *20th European Microwave Conf. Proc.*, vol. 2, Sept. 1990, pp. 1136–1141.
[9] M. Abouzahra and L. Lewin, "Theory and application of coupling between curved transmission lines," *IEEE Trans. Microwave Theory Tech.*, vol. MTT-30, pp. 1988–1995, 1982.
[10] M. Matsuhara and W. Watanabe, "Coupling of curved transmission lines and application to optical directional couplers," *J. Opt. Soc. Amer.*, vol. 65, no. 2, pp. 163–168, 1975.
[11] T. Trinh and R. Mittra, "Coupling characteristics of planar dielectric waveguides of rectangular cross section," *IEEE Trans. Micro-wave Theory Tech.*, vol. MTT-29, pp. 875–880, Sept. 1981.
[12] A. W. Snyder, "Coupled-mode theory for optical fibers," *J. Opt. Soc. Amer.*, vol. 62, pp. 1267–1277, 1972.
[13] S. L. Chuang, "A coupled mode formulation by reciprocity and a variational principle," *J. Lightwave Technol.*, vol. LT-5, no. 1, pp. 5–15, Jan. 1987.
[14] M. A. Mchenry and D. C. Chang, "Coupled-mode theory of two nonparallel dielectric waveguides," *IEEE Trans. Microwave Theory Tech.*, vol. MTT-32, no. 11, pp. 1469–1475, Nov. 1984.
[15] Y. Tomabechi and K. Matsumura, "Coupling characteristics of nonparallel dielectric waveguides," (in Japanese), *Trans. IEICE*, C-I, vol. J77-C-I, no. 2, pp. 57–63, Feb. 1994.
[16] K. Matsumura Y. Tomabechi, Y. Kogami, and J. H. Hwang, "Electromagnetic coupling between curved dielectric waveguides," in *24th European Microwave Conf. Proc.*, vol. 1, Sept. 1994, pp. 692–697.

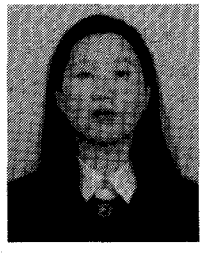

Qing Han (S'95) received the B.S. degree in electrical engineering from East China Institute of Engineering, Nanjing, China, in 1983, and the M.S. degree in electrical and electronic engineering from Utsunomiya University, Utsunomiya, Japan, in 1993. She is now studying for Doctor of Engineering degree at the Utsunomiya University.

She has engaged in research for dielectric resonators.

Yoshinori Kogami (M'95) was born in Tokyo, Japan, on July 23, 1964. He received the B.E., M.E. degrees in electrical engineering, and Ph.D. degree in production and information sciences from Saitama University in 1988, 1990, and 1993, respectively.

He is now a Research Associate in the Department of Electrical and Electronic Engineering, Utsunomiya University, Utsunomiya, Japan. He has engaged in research for dielectric resonators and filters.

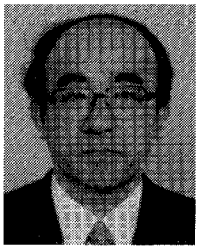

Yoshiro Tomabechi (M'83) received the B.S. and M.S. degrees in electrical engineering from Yamagata University, Yonezawa, Japan, in 1971 and 1973, respectively. He also received the Doctor of Engineering degree from Tohoku University Sendai, Japan in 1989.

From 1973 to 1991, he was a Research Associate of the Faculty of Engineering at Utsunomiya University. Since 1991, he has been an Associate Professor of the Faculty of Education at Utsunomiya University. His present research activity has been directed toward the analysis of wave guiding mechanism, especially the rectangular dielectric wave guide and the dielectric resonator.

Dr. Tomabechi is a Member of the Institute of Electronics, Information and Communication Engineers of Japan.

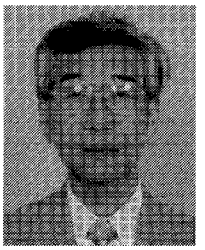

Kazuhito Matsumura (S'62–M'67–SM'86) was born in Yamanashi, Japan, on August 11, 1938. He received the B.S. degree in electrical engineering from Yamanashi University, in 1961. He also received the M.S. and Doctor of Engineering degrees in communication engineering from Tohoku University, Sendai, Japan, in 1964 and 1967, respectively.

From 1967 to 1970 he was a Research Associate, and from 1971 to 1972, an Associate Professor at Tohoku University. In 1973, he moved to Utsunomiya University, Utsunomiya, Japan, where he is now a Professor on the Faculty of Engineering. From 1976 to 1977 he was with the Technische Hochschule Darmstadt, Federal Republic of Germany, as a Guest Professor. His research works have been concerned with waveguiding mechanism and circuit components on the millimeter, sub millimeter and optical wave regions.

Dr. Matsumura is a Member of the Institute of Electronics, Information and Communication Engineers of Japan.